Homogeneous and mixed UF_6 clusters with Ar: Calculations of structures and vibrational spectra

T. A. Beu,[a] J. Onoe, and K. Takeuchi
The Institute of Physical and Chemical Research (RIKEN), Wako-shi, Saitama 351-0198, Japan

(Received 17 July 1998; accepted 11 August 1998)

A recently developed site–site intermolecular potential for UF_6, featuring exchange, dispersion, and electrostatic terms, is used to calculate minimum energy structures of homogeneous UF_6 clusters up to the decamer. The structures of mixed $(UF_6)_2$–Ar_n clusters are also calculated by adding appropriate interaction terms. The IR spectra corresponding to the determined cluster structures in the region of the ν_3 vibrational mode of the monomer (at 627.724 cm^{-1}) are calculated using a second-order line shift formalism, treating the anharmonic intramolecular force field and the intermolecular potential as a perturbation. The leading interaction mechanism responsible for the line shifts of the ν_3 mode is found to be the electrostatic one (implicitly the resonant dipole–dipole coupling). The theoretical spectra are shown to satisfactorily describe the peaks around 623, 632, and 640 cm^{-1} found in the recently measured Fourier transform IR spectra in a continuous supersonic Laval nozzle flow and attributed to the clusters formed by UF_6. © *1998 American Institute of Physics.* [S0021-9606(98)00943-X]

I. INTRODUCTION

The formation of UF_6 clusters is considered to have a detrimental effect on the selectivity in molecular laser isotope separation with the supersonic expansion technique through the frequency shift it produces in the IR absorption of the ν_3 vibrational mode of the UF_6 monomer at 627.724 cm^{-1}. Despite the importance of the elucidation of the formation kinetics and of the IR spectrum of the UF_6 clusters, there have been no published results on this subject for a long time. In exchange, the last two decades have been quite fruitful experimentally and theoretically regarding the investigation of the less demanding SF_6 system,[1–8] used to establish adequate experimental and theoretical methodologies.

The recent Fourier-transform infrared (FTIR) spectroscopy measurements of Tanimura *et al.*[9,10] are the only published experimental data concerning the UF_6 cluster formation and are used as an experimental counterpart for our calculations. The FTIR spectroscopic measurements in supersonic free jets have the advantage of a wider spectral coverage than any laser system, allowing for simultaneous observation of the spectra for both the monomer and its clusters.[9,11] However, the lack of a size selection mechanism makes interpretation of the FTIR spectra quite difficult.

Recently we have published a detailed study (hereafter referred to as ''paper I'') on the structures and IR spectra of homogeneous UF_6 clusters up to the hexamer, which was based on a new site–site intermolecular potential model comprising exchange, dispersion, electrostatic, and induction terms.[12] Basically, in establishing the site–site intermolecular potential of UF_6 we followed the pattern previously employed for the construction of the SF_6 intermolecular potential.[7] The effective charges assigned to the U atom and the six additional ''electronic'' sites situated on the U–F bonds have been chosen such as to account for the observed vibrational transition dipole moment of the UF_6 monomer. All the coefficients of the exp-6 part of the potential for uranium have been determined by fitting the calculated temperature dependence of the second virial coefficient of UF_6 to the experimental evidence.

To calculate the IR spectra of the UF_6 clusters found in the region of the ν_3 mode, a degenerate second-order perturbation approach for frequency shifts was used, treating the anharmonic contributions to the intramolecular force field and the intermolecular potential as a quantum mechanical perturbation. The formalism generalizes earlier work[13] and has been successfully applied to the calculation of IR spectra for small SF_6 clusters as well.[7,8] Among the contributions to the line shifts of the UF_6 clusters, the vibrational dipole–dipole interaction was found to be dominant.[12] The calculated spectra explain satisfactorily the available experimental FTIR spectra of UF_6 seeded in Ar, excepting one broad peak around 610 cm^{-1}. The overall better agreement of the results obtained neglecting induction over those including it was apparent, probably due to the insufficiently accurate available polarizabilities.

The purpose of the present paper is to extend the knowledge gained by the investigations reported in paper I with results concerning minimum energy structures and the corresponding IR spectra for homogeneous $(UF_6)_M$ clusters up to the decamer and mixed $(UF_6)_2$–Ar_n clusters with up to 50 Ar atoms. The inclusion of the treatment of the mixed clusters of UF_6 with Ar is intended to elucidate the origin of the unexplained peak around 610 cm^{-1}, revealed by the FTIR measurements on UF_6 seeded in Ar.[9,10]

In the case of the homogeneous clusters we have used the intermolecular potential of paper I including exchange,

[a]On leave from the University of Cluj-Napoca, Department of Theoretical Physics, 3400 Cluj-Napoca, Romania.

dispersion, and electrostatic terms, while for the mixed clusters specific terms have been added to account for the Ar–UF_6 and Ar–Ar interactions, based on the most accurate potential models available in the literature.

In Sec. II A we give a brief outline of our previously published perturbation approach for calculating the frequency shifts. The potential model we employ to determine the geometrical structures and line shifts of the clusters is described in Sec. II B. Section III A is devoted to a description of the structures obtained for the homogeneous UF_6 clusters ranging from heptamer to decamer and for the mixed $(UF_6)_2$–Ar_n clusters with $n=2-50$. Based on the obtained configurations, the results of our frequency shift calculations, both for the homogeneous and mixed clusters, are given in Sec. III B.

II. THEORETICAL MODEL

A. Frequency shift approach

According to the perturbation formalism presented in paper I, for a cluster formed of M identical molecules, the first-order frequency shifts $\Delta\nu_{ni}^{(1)}$ relative to a particular vibrational mode n of the monomer directly result from the eigenvalue problem

$$\sum_{n'\in\Gamma}\sum_{i'=1}^{M}\left[\frac{1}{2}\frac{\partial^2 U}{\partial q_{ni}\partial q_{n'i'}}-hc\Delta\nu_{ni}^{(1)}\delta_{nn'}\delta_{ii'}\right]c_{n'i',ni}=0,\qquad i=1,2,\ldots,M. \tag{1}$$

The matrix elements are expressed in terms of the curvature of the intermolecular potential U, which, in the case of mixed clusters, also includes the interactions with the different molecular or atomic species. q_{ni} is the position operator associated with the normal mode n of molecule i. In the degenerate case, both n and n' belong to the same subspace Γ of the considered normal mode, while for a nondegenerate mode, $n\equiv n'$.

The second-order line shifts can be expressed as

$$\Delta\nu_{ni}^{(2)}=\sum_{n',n''\in\Gamma}\sum_{i',i''}c_{n'i',ni}c_{n''i'',ni}^{*}\Delta\nu_{n'i',n''i''}^{(2)},$$

where

$$\begin{aligned}\Delta\nu_{n'i',n''i''}^{(2)}&=-\frac{\delta_{i'i''}}{2hc}\sum_{r}\frac{1}{\omega_r}\frac{\partial U}{\partial q_{ri'}}\phi_{n'n''r}+\frac{1}{4(hc)^2}\\&\times\sum_{r\notin\Gamma}\sum_{m}\frac{1}{\omega_n-\omega_r}\frac{\partial^2 U}{\partial q_{n'i'}\partial q_{rm}}\frac{\partial^2 U}{\partial q_{n''i''}\partial q_{rm}}-\frac{1}{4(hc)^2}\\&\times\sum_{r}\sum_{m}\frac{1}{\omega_n+\omega_r}\frac{\partial^2 U}{\partial q_{n'i'}\partial q_{rm}}\frac{\partial^2 U}{\partial q_{n''i''}\partial q_{rm}}.\end{aligned}$$

Here ω_n and $\phi_{n'n''r}$ are harmonic frequencies and cubic force constants, respectively. The first term of $\Delta\nu_{n'i',n''i''}^{(2)}$ is cast under a more compact (however less explicit) form, as compared to our previous publications.[7,12] The calculation details of the cubic force constants, $\phi_{n'n''r}$, and of the intermolecular potential derivatives with respect to the normal coordinates can be found in Refs. 7 and 12 and are based on the G-F method of Wilson[14] and the L-tensor formalism of Hoy, Mills, and Strey.[15]

B. Intermolecular potential

In calculating the structures and the corresponding vibrational frequency shifts for the homogeneous UF_6 clusters we have used the UF_6–UF_6 intermolecular potential previously introduced in paper I under the name ''potential I,'' which comprises exchange, dispersion, and electrostatic terms. Since the induction interaction with the presently available polarizabilities was found to yield irrelevant results in describing the UF_6 clusters up to the hexamer, we have no longer considered this contribution. Depending on the relative atom positions, the developed site–site potential naturally depends on the internal monomer vibrational coordinates.

In the case of the mixed $(UF_6)_2$–Ar_n clusters, we have modeled the Ar–UF_6 interaction by an anisotropic potential similar to that introduced by Eichenauer and Le Roy for Ar–SF_6.[16] It is represented as a sum over Ar–U and Ar–F pair potentials. Explicitly, the interaction between a particular Ar atom and one of the F atoms of an UF_6 molecule, is given by

$$U_{\mathrm{Ar-F}_l}(r_l,\theta_l)=A[1+pP_2(\cos\theta_l)]e^{-br_l}-\sum_{n=3}^{5}\left[1-e^{-br_l}\sum_{k=0}^{2n}\frac{(br_l)^k}{k!}\right]\frac{C_{2n}}{r_l^{2n}}.$$

Here $\mathbf{r}_l=\mathbf{r}_{\mathrm{Ar}}-\mathbf{r}_{\mathrm{F}_l}$ is the relative position vector of the Ar atom with respect to the F atom and θ_l is the angle subtended by vectors $\mathbf{r}_l$ and $\mathbf{r}_{\mathrm{F}_l}-\mathbf{r}_{\mathrm{U}}$, the latter defining the relative position of the F atom with respect to the U atom. $P_2(\cos\theta_l)=(1/2)(3\cos^2\theta_l-1)$ is the second-order Legendre polynomial. The parameters we employed for the Ar–F interaction are those reported by Eichenauer and Le Roy.[16]

For the Ar–U interaction we consider a similar pair potential, except for the absence of the first term and the sole dependence on the Ar–U distance $r=|\mathbf{r}_{\mathrm{Ar}}-\mathbf{r}_{\mathrm{U}}|$:

$$U_{\mathrm{Ar-U}}(r)=-\sum_{n=3}^{5}\left[1-e^{-br}\sum_{k=0}^{2n}\frac{(br)^k}{k!}\right]\frac{C_{2n}}{r^{2n}}.$$

Since there are no dispersion coefficients for this interaction available in the literature, we have scaled proportionally the corresponding coefficients of the Ar–S interaction as reported by Eichenauer and Le Roy, such as to fit the isotropic UF_6–Ar potential of Schneider *et al.*[17] along directions bisecting the solid angles between three neighboring U–F bonds. The resulting parameters are listed in Table I.

To describe the Ar–Ar interaction we have used the elaborate potential of Aziz and Slaman,[18] which incorporates the most accurate available C_6 dispersion coefficients and was additionally fitted to the experimental vibration–rotation band system, viscosity, and second virial data. The functional form of this potential is

TABLE I. Parameters of the atom–atom Ar–UF_6 potential model.

	Ar–U	Ar–F
A (eV)		15.7
p		−0.675
b ($^{-1}$)	4.00	4.23
C_6 (eV^6)	101.20	5.52
C_8 (eV^8)	883.16	0.00
C_{10} (eV^{10})	7298.00	0.00

$$U_{\mathrm{Ar-Ar}}(r)=\epsilon\left[A^*\ \exp(-\alpha^*x+\beta^*x^2)-F(x)\sum_{j=0}^{2} c^*_{2j+6}/x^{2j+6}\right],$$

being expressed in terms of the dimensionless coordinate $x=r/r_m$ and with the damping function $F(x)$ defined by

$$F(x)=\begin{cases}\exp[-(D/x-1)^2], & x<D\\ 1, & x\geqslant D.\end{cases}$$

All relevant data for the description of the Ar–Ar interaction can be found in Table 1 of Ref. 18.

III. RESULTS

A. Cluster structures

In order to determine the equilibrium structures of the homogeneous $(UF_6)_M$ clusters, the molecules have been considered rigid and the intermolecular potential has been minimized with respect to their relative positions and orientations, specified by the Cartesian coordinates of their center of masses and the corresponding Euler angles, respectively. To ensure that the global minimum is obtained, we have performed for each cluster size roughly as many thousands of minimizations as given by the cluster size, starting from randomly chosen initial configurations. In the case of the mixed $(UF_6)_2$–Ar_n clusters, the Ar positions have been treated as additional degrees of freedom, each new Ar atom being initially placed in random positions about the equilibrium structure obtained for the previous number of Ar atoms. For the mixed clusters, up to 30 000 minimizations have been necessary to yield the lowest energy configurations.

We have gathered in Table II the results of our structure calculations for homogeneous $(UF_6)_M$ clusters up to the decamer, in terms of the binding energy, symmetry, and average distance of the nearest U atoms, d_{UU}, meant to be an indication about the cluster ''compactness.'' For all cluster sizes the data for the most stable isomer are listed. The results for the clusters up to the hexamer have been extensively discussed in paper I, where, except for the hexamer itself, the lowest energy configurations for all cluster sizes have been found to show remarkable symmetry properties. It was confirmed that UF_6 forms true van der Waals clusters, mainly bound by the dispersion attraction.

TABLE II. Calculated $(UF_6)_M$ cluster structures for the energetically most stable isomers. E represents the total binding energy (in kJ/mol), and d_{UU} is the average U–U distance (in Å).

M	E	d_{UU}	Symmetry
2	−8.66	5.381	D_{2d}
3	−23.46	5.487	D_3
4	−40.77	5.672	C_3
5	−62.99	5.673	C_{3h}
6	−86.17	5.632	
7	−109.82	5.633	
8	−134.80	5.585	
9	−158.84	5.604	C_2
10	−182.96	5.566	

We have depicted in Fig. 1 the lowest energy heptamer. The considered isomer has a distorted bipyramidal structure with a fivefold axis, along which it is viewed. The average U–U distance (5.633) approximately preserves the value featured by the hexamer and is somewhat larger than the average S–S distance (5.18) found in Ref. 8 for the SF_6 heptamer, which has a quite similar structure. In fact, the larger U–U distances as compared to the corresponding S–S distances for the clusters of the same size appears to be a general characteristic and is obviously caused by the more voluminous uranium atoms.

Figure 2 shows the top and side views of the energetically most stable octamer. The octamer can be regarded as a superposition of four reciprocally orthogonal sandwiched dimers. The very compact octamer is also characterized by a decrease of the average d_{UU} distance as compared to the lowest energy heptamer.

Quite surprisingly, the most stable nonamer (Fig. 3) is again symmetric, dissimilar to the heptamer, octamer, and decamer. It has C_2 symmetry, consisting of two orthogonal dimers in the near plane, a ring made of two parallel dimers, and an isolated monomer in the far plane. As concerns the average U–U distance, the nonamer is less compact than the octamer.

The lowest energy decamer, depicted as top and side views in Fig. 4, apparently exhibits a regular structure, being composed of two fourfold rings in the middle plane, and two isolated monomers in the near and the far plane, respectively.

The plot of the incremental binding energy E_M-E_{M-1} of the most stable isomers as a function of the size M (Fig. 5) offers interesting informations. The overall saturation tendency of the incremental binding energy with increasing cluster size is apparent, meaning that, for larger clusters, each added monomer enters a host structure in which it significantly interacts only with the closest neighbors. Through the large energy increment, the octamer departs to some extent from the general behavior and this can be correlated also with its low average U–U distance, reflection of an enhanced compactness.

The structure calculations for the mixed $(UF_6)_2$–Ar_n clusters being extremely time consuming, we have confined our investigations to clusters with an even number of Ar atoms $n=2-50$. We mention that this range is consistent with the mole fraction of 0.08 used in the FTIR experiments reported by Tanimura *et al.*[9] and which are used in Sec. III B as a counterpart to our IR-spectrum calculations. The obtained cluster structures, along with the corresponding binding energies, are depicted in Fig. 6 for some selected values

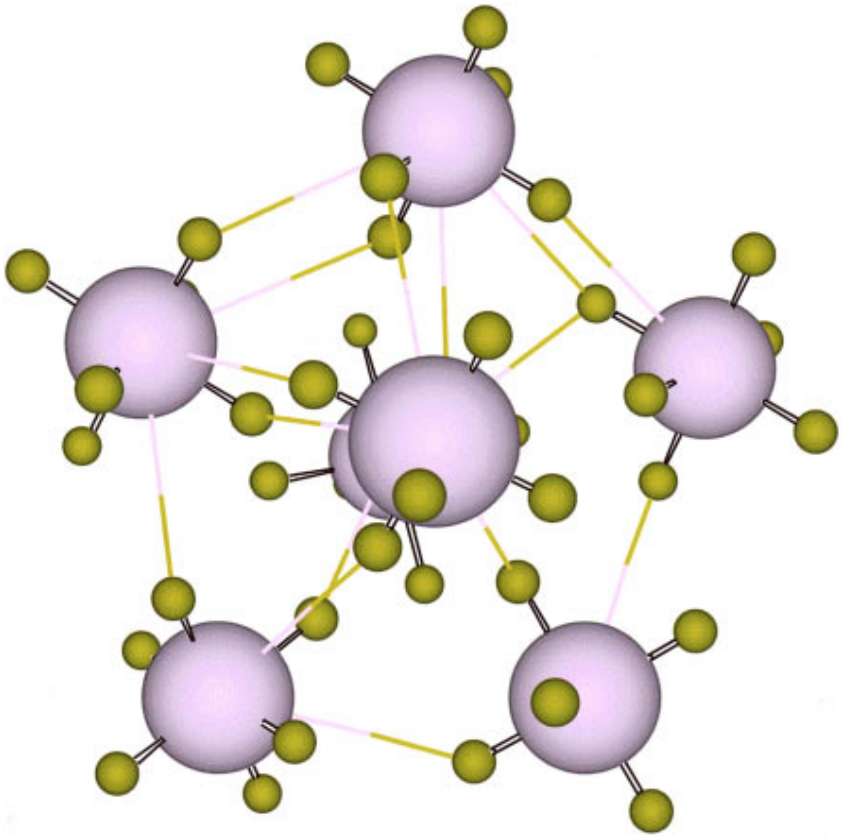

FIG. 1. Geometrical structure of the lowest energy UF_6 heptamer.

of n. All structures are viewed along the UF_6 ''dimer'' axis. As it can be easily seen, the configurations with n less than 16 tend to form a structure featuring open cells about the UF_6 dimer axis. Starting with $n=16$, however, this trend is abandoned, and an energetically more favorable structure with closed cells on one side of the UF_6 dimer is formed, which is continued up to $n=50$. The side views of $(UF_6)_2$–Ar_{16} and $(UF_6)_2$–Ar_{38} included in Fig. 7 clearly show the closed Ar

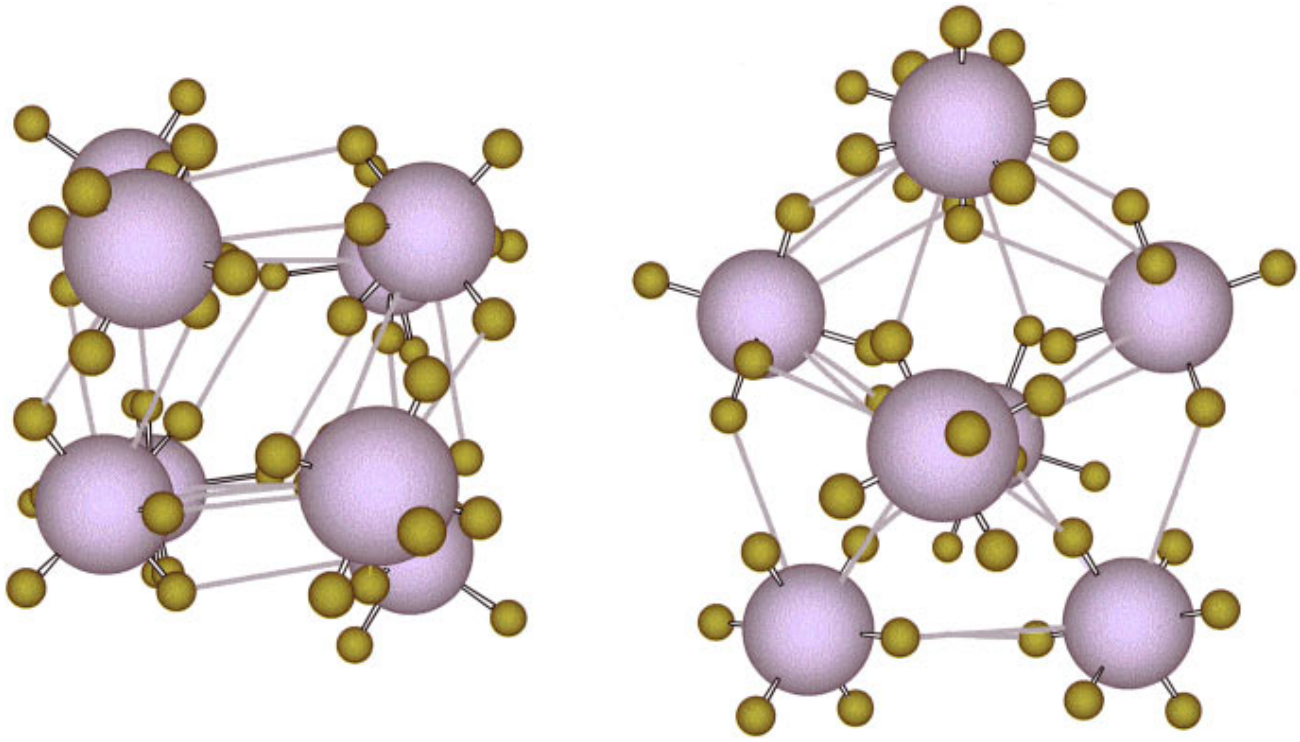

FIG. 2. Top and side views of the lowest energy UF_6 octamer.

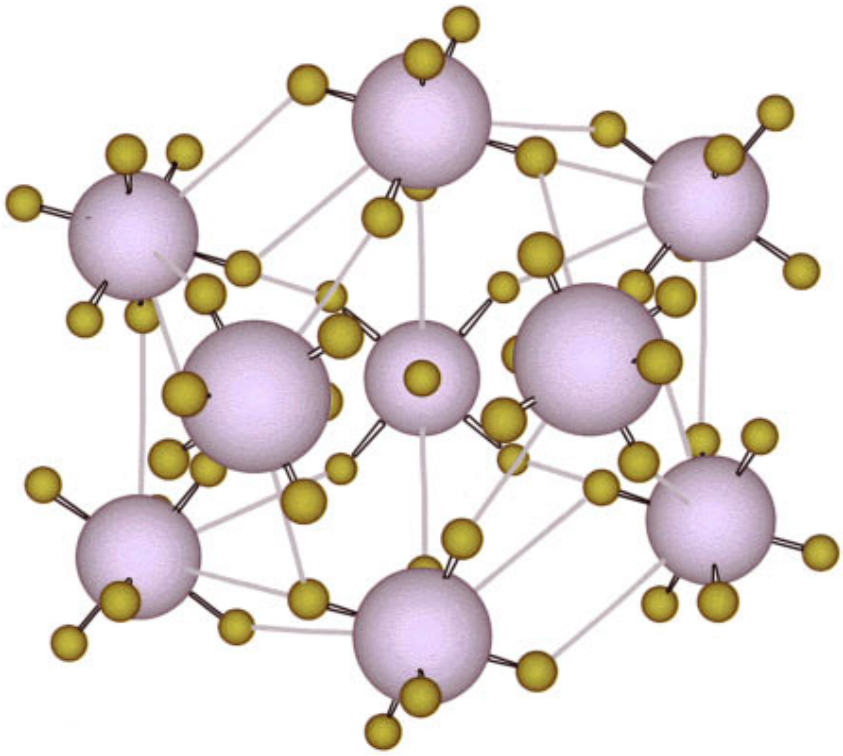

FIG. 3. Geometrical structure of the lowest energy UF_6 nonamer.

atom shells which are gradually formed about the UF_6 dimer axis. As opposed to the $(SF_6)_2$–Ar_n clusters investigated in Ref. 8, for which the SF_6 dimer is quite uniformly surrounded by the Ar atoms, in the case of the $(UF_6)_2$–Ar_n clusters the UF_6 dimer is rather ''expelled'' from the cluster structure, with the Ar atoms roughly organized on one side. This different behavior can be straightforwardly explained by the less attractive Ar–U interaction, evidenced by its

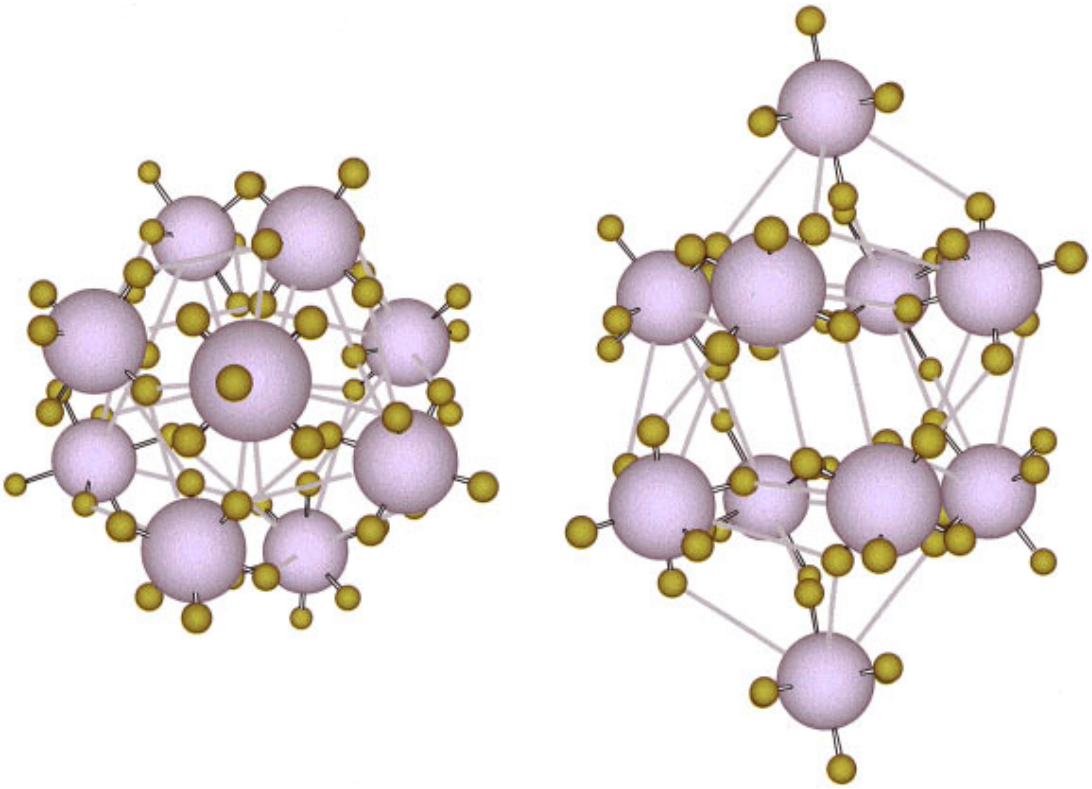

FIG. 4. Top and side views of the lowest energy UF_6 decamer.

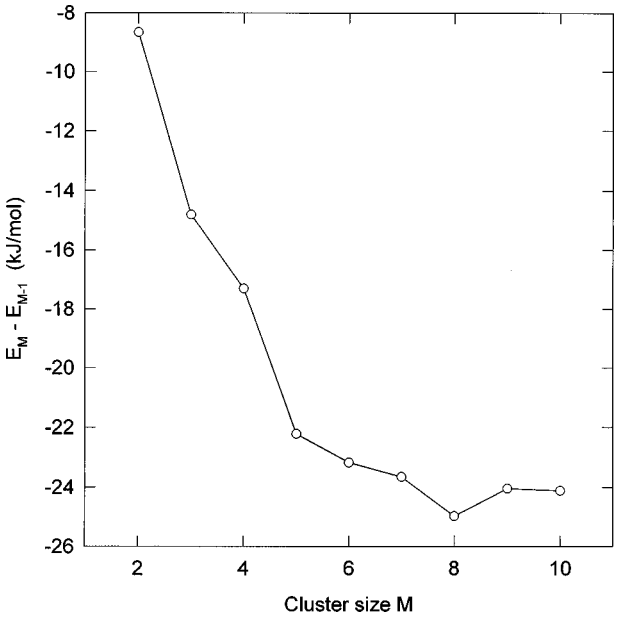

FIG. 5. Incremental binding energy of homogeneous $(UF_6)_M$ clusters.

smaller dispersion coefficients (given in Table I) as compared to those for the Ar–S interaction (reported in Ref. 16).

The binding energy E_n of the most stable $(UF_6)_2$–Ar_n isomer decreases smoothly as a function of the Ar atom number n, as can be seen from Fig. 8. In order to evidence the quasicontinuum of stable isomer states in the vicinity of the most stable configuration, we have plotted the binding energy for the second lowest isomer, too, and this curve is practically indistinguishable from the one for the most stable configurations. The closeness of the two curves indicates that the lowest energy configurations have actually been found. The corresponding incremental binding energy as a function of the Ar atom number n is plotted in Fig. 9. The incremental binding energy is defined as $E_n - E_{n-2}$ since only even values for n have been considered. For higher numbers of Ar

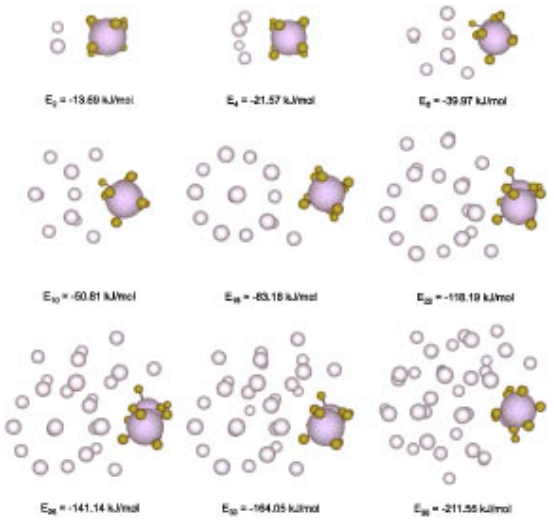

FIG. 6. Geometrical structures of the most stable $(UF_6)_2$–Ar_n clusters, for several even values of n, viewed along the UF_6-dimer axis. For each configuration, the total binding energy, E_n, is indicated.

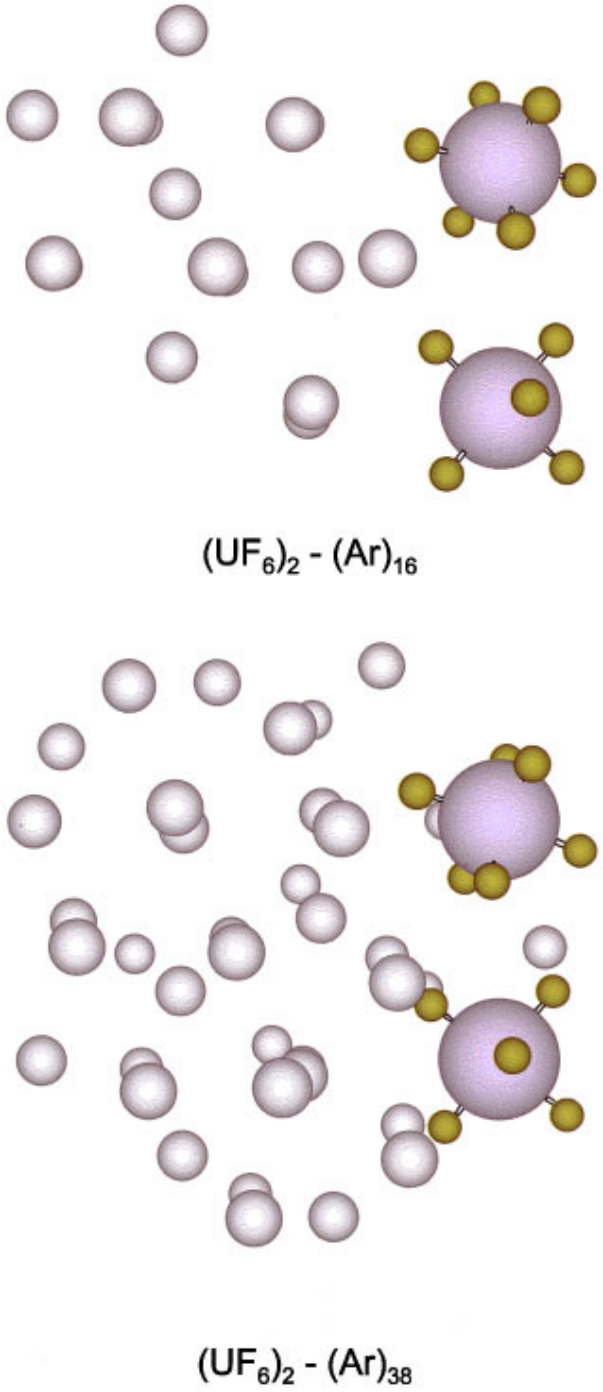

FIG. 7. Side view of the lowest energy $(UF_6)_2$–Ar_{16} and $(SF_6)_2$–Ar_{38} clusters.

atoms, the saturation tendency of the overall decreasing behavior becomes apparent. The oscillations of the plot corresponding to the most stable isomers are closely followed by those for the second lowest isomers, suggesting, as before, the convergence of our search procedure for the implied minimum energy configurations.

B. Frequency shifts

The band shift calculations for both the homogeneous and the mixed UF_6 clusters deal with the fundamental excitation of the ν_3 vibrational mode of the UF_6 monomer at 627.724 cm^{-1}.

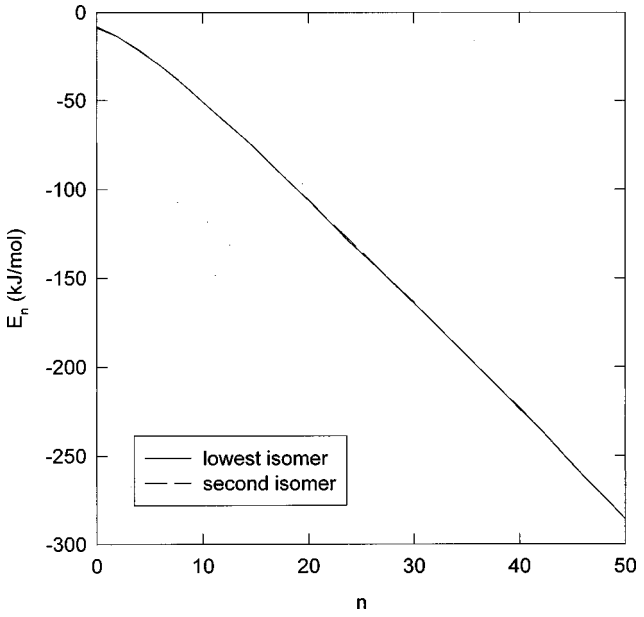

FIG. 8. Binding energy of the lowest and second lowest energy configurations of the $(UF_6)_2$–Ar_n clusters.

The mutual interaction of the monomers within the clusters causes the ν_3 vibrational mode to be split up into redshifted parallel bands (∥) and blueshifted perpendicular bands (⊥). The calculated second-order corrections of the line shifts typically amount to less than 1.5 cm^{-1}. Such small corrections are a result of the reduced anharmonicity of the considered vibrational mode, but they are also due to the small intermolecular potential curvature in the vicinity of the global minimum (the mixed second-order derivatives $\partial^2 U/\partial q_{ni}\partial q_{rm}$ are of the order of 0.5 cm^{-1}).

Performing separate calculations for the individual contributions to the total intermolecular potential, the vibrational dipole–dipole interaction was found to be mainly responsible for the frequency shifts. By contrast, the effects of the exchange and dispersion couplings have turned out to be negligible, even though they are determining for the cluster structures.[12] As discussed in paper I, up to the hexamer the induction interaction contributes approximately 17% to the total frequency shifts. However, leading through systematic redshifts to a poorer agreement with the experimental FTIR measurements (presumably due to inaccurate polarizabilities), induction was no longer included in the present work.

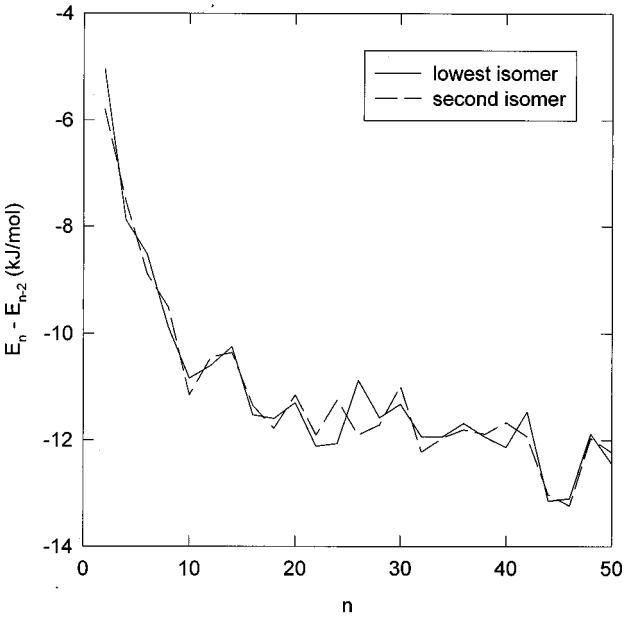

FIG. 9. Incremental binding energy of the lowest and second lowest energy configurations of the $(UF_6)_2$–Ar_n clusters.

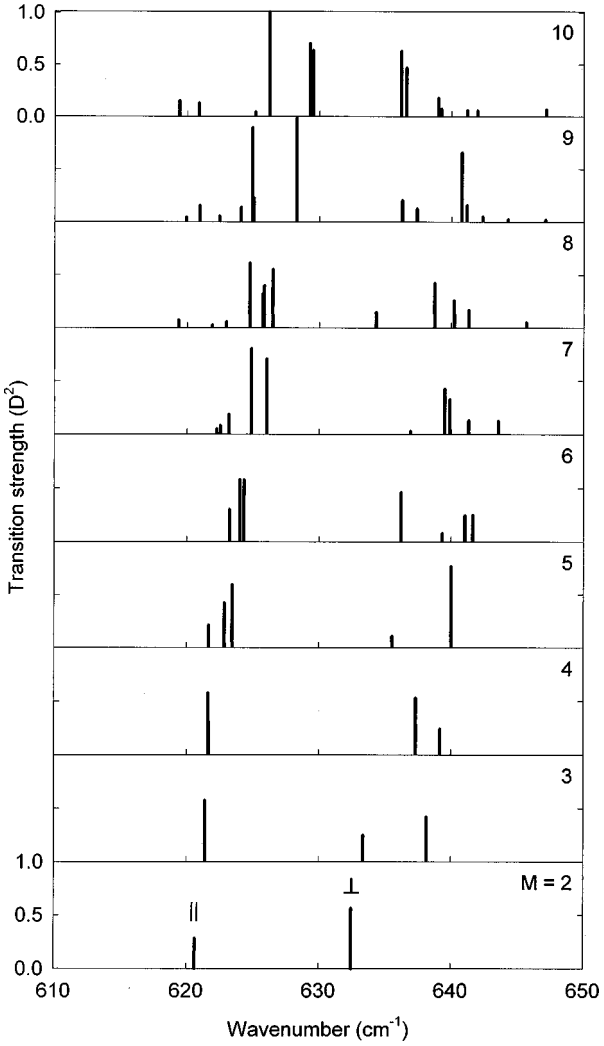

FIG. 10. Calculated stick spectra of homogeneous $(UF_6)_M$ clusters from dimer to decamer. For all cluster sizes, the most stable isomer is being considered.

Figure 10 shows the stick spectra of the UF_6 clusters up to the decamer. The lines have been denoted according to the sign of the frequency shift: with ∥ for redshifted lines and with ⊥ for the blueshifted ones. As it can be easily noticed, the red boundary of the spectra seems to be quite insensitive to the cluster size, preserving its value of about 620 cm^{-1} with increasing cluster size. As for the ''perpendicular'' lines, they gradually move toward higher frequencies, however showing a saturation tendency.

By virtue of the symmetry properties of the clusters, the splitting pattern up to the pentamer remains quite simple.

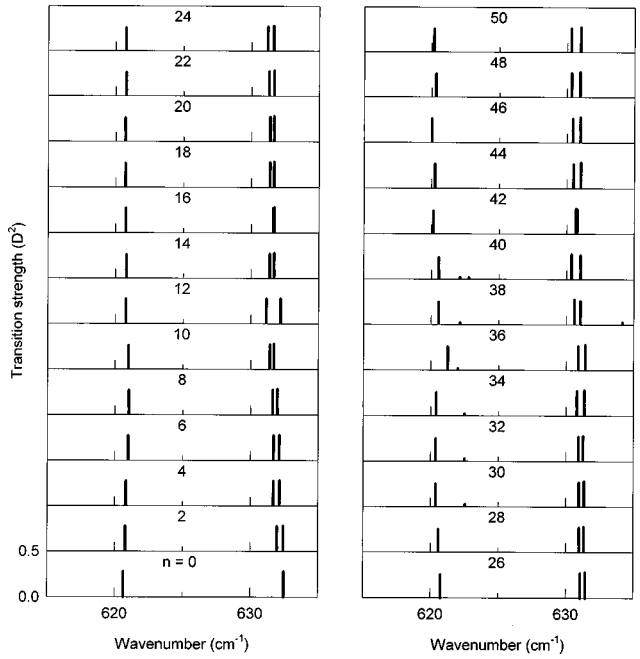

FIG. 11. Calculated stick spectra of $(UF_6)_2$–Ar_n clusters. For all cluster sizes, the most stable isomer is being considered.

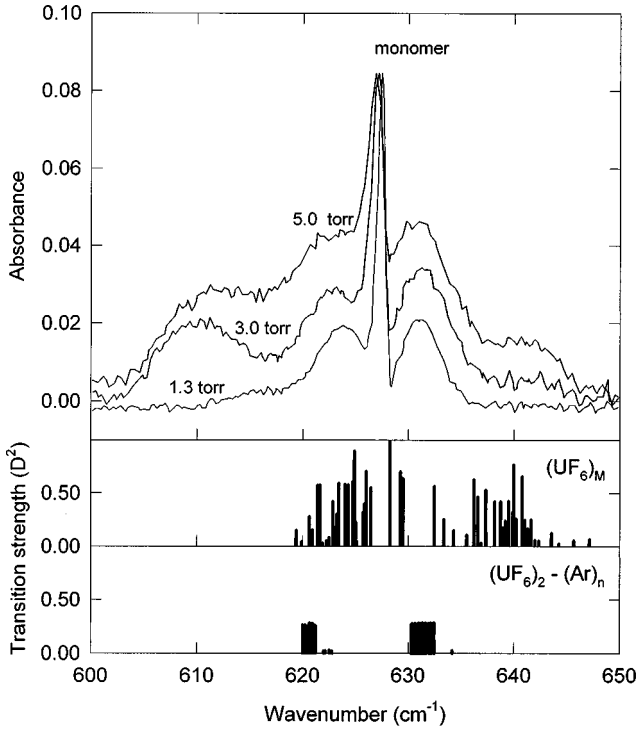

FIG. 12. FTIR spectrum of UF_6 clusters seeded in Ar and calculated stick spectra of $(UF_6)_{2\text{-}10}$ and $(UF_6)_2$–$Ar_{2\text{-}50}$ clusters.

From the hexamer onward, the lack of a well-defined geometrical symmetry and the increase of the number of UF_6 monomers in nonequivalent positions causes the stick spectra to be much less structured. The nonamer appears, however, to be an exception among the larger of the considered clusters with its three distinctly individualized lines (the others being of much smaller intensity). This is obviously a consequence of its symmetrical structure, emphasized in Sec. III A.

By comparing the stick spectra of the homogeneous UF_6 clusters with those of the homogeneous SF_6 clusters reported in Fig. 10 of Ref. 8, one can notice the same overall trend of the spectral lines with increasing cluster size, but an inferior average splitting corresponding to the UF_6 clusters (approximately 15 cm^{-1} as compared to 23 cm^{-1}). Since the dominant interaction was proven to be the vibrational dipole–dipole interaction, this finding can be directly correlated with the experimental values of the transition dipole moment for the UF_6 and SF_6 monomers: 0.385 and 0.437 D, respectively.[19,20]

The behavior of the calculated stick spectra for the mixed $(UF_6)_2$–Ar_n clusters, depicted in Fig. 11 for $n=2$–50, is just opposed to that of the spectra for the homogeneous clusters: With increasing cluster size, the lines are systematically redshifted. A surprising finding is, however, that the lines for $(UF_6)_2$–Ar_{50} are very little shifted with respect to those of the homogeneous UF_6 dimer (by less than 2 cm^{-1}). On the other hand, the total splitting for the $(UF_6)_2$–Ar_n clusters is very little sensitive to the cluster size. Similar results have been obtained also for the $(SF_6)_2$–Ar_n clusters:[8] The total splitting was found to have an almost nonvarying value (about 23 cm^{-1}) from the homogeneous SF_6 dimer up to $(SF_6)_2$–Ar_{50}, even though the lines of the latter are redshifted by approximately 5 cm^{-1}.

An explanation of the larger shifts in the case of the $(SF_6)_2$–Ar_n clusters as compared to those for the $(UF_6)_2$–Ar_n clusters is offered by the qualitatively different arrangement of the Ar atoms within the two species of mixed clusters, evidenced in Sec. III A. Whereas in the $(SF_6)_2$–Ar_n clusters the Ar atoms wrap the SF_6 dimer in a cell-like structure, the UF_6 dimer is eliminated from the structure formed by the Ar atoms, which brings about a diminished redshifting interaction of the UF_6 monomers with the Ar atoms.

Tanimura and co-workers have studied the clustering of UF_6 seeded in Ar in a continuous supersonic Laval nozzle flow and have investigated the clustering onset temperature and density of UF_6 by FTIR spectroscopy.[9,10] These are in fact the only available experimental data concerning the UF_6 clusters. The same experimental technique was also employed in our FTIR spectroscopy studies on the SF_6 clustering.[8,21]

Figure 12 shows the FTIR spectra of the ν_3 band of UF_6 seeded in Ar at a mole fraction of 0.08 mol/mol and total pressures of 1.3, 3.0, and 5.0 Torr. The obtained spectra are shown in the upper panel of Fig. 12. All three spectra clearly feature the *P*, *Q*, and *R* branches of the UF_6 monomer in the range between 620 and 640 cm^{-1}.

Whereas the peaks around 623 and 632 cm^{-1}, besides the *P* and *R* branches of the monomer, also contain contributions from the cluster spectra, the peak at 640 cm^{-1} is clearly due to the presence of the UF_6 clusters alone, since it is absent from the spectrum at 1.3 Torr. This can be explained by inspecting the middle panel of Fig. 12, which shows the calculated stick spectra of the homogeneous UF_6 clusters up to the decamer. Except for the dimer, the perpendicular blueshifted lines of all cluster sizes contribute to the

broad and flat peak located around 640 cm^{-1}. The clusters larger than the dimer are consequently formed only at total pressures above 3.0 Torr. In the blueshifted band around 632 cm^{-1} there are dominantly contributions from the dimer and the trimer, while in the redshifted band around 623 cm^{-1}, there are contributions from all cluster sizes. Our calculations for homogeneous UF_6 clusters did not evidence any line corresponding to the peak around 610 cm^{-1}, clearly separated in the FTIR spectrum at 3.0 Torr.

The lower panel of Fig. 12 displays the calculated stick spectra of the $(UF_6)_2$–Ar_n clusters with $n=2-50$. The spectral lines corresponding to the higher number of Ar atoms are shifted to the left of each of the two groups and, consequently, the lines for $n>50$ are expected to continue this trend. However, the overall redshift of these lines is by far too small to offer an explanation of the peak at 610 cm^{-1}. Even though the redshifting behavior is likely to characterize also the mixed clusters consisting of more than two UF_6 monomers, it seems improbable for them to yield large enough frequency shifts to explain this peak.

IV. CONCLUSIONS

The present work continues the investigations initiated in paper I (Ref. 12), concerning the structure and IR spectra of homogeneous and mixed clusters involving UF_6 molecules and Ar atoms. The homogeneous UF_6 clusters from dimer to hexamer have been extensively analyzed in paper I and the new results rather refer to the homogeneous clusters from heptamer to decamer and to the mixed $(UF_6)_2$–Ar_n clusters.

One of the main results of the reported work is a new site–site intermolecular potential for UF_6. The effective charges assigned to the interaction sites have been determined consistently with the observed vibrational transition dipole moment of the UF_6 monomer. The exchange and dispersion coefficients for the individual atomic species have been fitted to the experimental temperature dependence of the second virial coefficient.

The found minimum energy structures for the homogeneous clusters have been analyzed in terms of their binding energy, incremental binding energy, symmetry properties, and average U–U distance, as a measure of the cluster ''compactness.'' Whereas the clusters up to the pentamer exhibit well-defined symmetries, the larger ones generally lack such properties. Among the larger clusters the nonamer again shows a symmetric structure. It is confirmed that UF_6 forms true van der Waals clusters, mainly bound by the dispersion attraction, the effect of the induction interactions being negligible.

By adding appropriate terms to describe the Ar–UF_6 and Ar–Ar interactions, a new potential energy surface for the mixed $(UF_6)_2$–Ar_n clusters has been built based on the UF_6–UF_6 intermolecular potential. In the $(UF_6)_2$–Ar_n clusters the Ar atoms form a cell-like structure with closed shells, from which the UF_6 dimer appears to be ''expelled.''

A previously published degenerate second-order perturbation formalism is used to calculate the IR spectra of the found UF_6 clusters (both homogeneous and mixed) in the region of the ν_3 vibrational mode. Among the contributions to the line shifts, those attributed to the vibrational dipole–dipole interaction are found to be dominant. The calculated stick spectra compare reasonably well with the available experimental FTIR spectra, allowing for a consistent explanation of the peaks located around 623, 632, and 640 cm^{-1}. It is noteworthy that this agreement is achieved despite the absence from the literature of size-selected high-resolution cluster spectra, which could be used to validate the UF_6–UF_6 intermolecular potential. Unfortunately, under the given circumstances the calculated spectra of neither the homogeneous nor the mixed clusters provide an explanation of the supplementary experimental peak located around 610 cm^{-1}. Further work is necessary to elucidate its origin.

[1] J. Geraedts, S. Stolte, and J. Reuss, Z. Phys. A **304**, 167 (1982); J. Geraedts, M. Waayer, S. Stolte, and J. Reuss, Faraday Discuss. Chem. Soc. **73**, 375 (1982).
[2] M. Snels and R. Fantoni, Chem. Phys. **109**, 67 (1986); M. Snels and J. Reuss, Chem. Phys. Lett. **140**, 543 (1987).
[3] F. Huisken and M. Stemmler, Chem. Phys. **132**, 351 (1989).
[4] B. Heijmen, A. Bizzarri, S. Stolte, and J. Reuss, Chem. Phys. **132**, 331 (1989).
[5] J. W. I. van Bladel and A. van der Avoird, J. Chem. Phys. **92**, 2837 (1989).
[6] A. Boutin, J.-B. Maillet, and A. H. Fuchs, J. Chem. Phys. **99**, 9944 (1993); A. Boutin, B. Rousseau, and A. H. Fuchs, Chem. Phys. Lett. **218**, 122 (1994).
[7] T. A. Beu and K. Takeuchi, J. Chem. Phys. **103**, 6394 (1995).
[8] T. A. Beu, Y. Okada, and K. Takeuchi, J. Chem. Phys. (submitted).
[9] S. Tanimura, Y. Okada, and K. Takeuchi, J. Phys. Chem. **100**, 2842 (1996).
[10] Y. Okada, S. Tanimura, H. Okamura, A. Suda, H. Tashiro, and K. Takeuchi, J. Mol. Struct. **410-411**, 299 (1997).
[11] J. A. Barnes and T. E. Gough, Chem. Phys. Lett. **130**, 297 (1986); J. Chem. Phys. **86**, 6012 (1987).
[12] T. A. Beu, J. Onoe, and K. Takeuchi, J. Chem. Phys. **106**, 5910 (1997).
[13] T. A. Beu, Z. Phys. D **31**, 95 (1994).
[14] E. B. Wilson, J. C. Decius, and P. C. Cross, *Molecular Vibrations* (McGraw–Hill, New York, 1955).
[15] A. R. Hoy, I. M. Mills, and G. Strey, Mol. Phys. **24**, 1265 (1972).
[16] D. Eichenaueer and R. J. Le Roy, J. Chem. Phys. **88**, 2898 (1988).
[17] B. Schneider, A. M. Boring, and J. S. Cohen, Chem. Phys. Lett. **27**, 577 (1974).
[18] R. A. Aziz and M. J. Slaman, Mol. Phys. **58**, 679 (1986).
[19] K. Kim, R. S. McDowell, and W. T. King, J. Chem. Phys. **73**, 36 (1980).
[20] K. C. Kim and W. B. Person, J. Chem. Phys. **74**, 171 (1981).
[21] Y. Okada, T. A. Beu, and K. Takeuchi (unpublished).